Supporting Information

Spent shell as calcium source constructing calcium vanadate for high-performance Zn-ion batteries

1. Experiment section

1.1 Synthesis of cathode materials

The CaV_3O_7 nanomaterials were prepared via a one-step hydrothermal method. 0.526 g of citric acid monohydrate ($C_6H_{10}O_8$) was poured into 20 mL of deionized (DI) water for stirring 5 min. 2.0 g of oyster shell powder was added into the above solution. The obtained mixing solution was stirred until the soluble matter was dissolved completely and filtered to obtain solution A. 0.4095 g of NH_4VO_3 was dissolved in 15 mL of DI water at 75 °C with magnetic stirring to obtain solution B. And then, the solution A was slowly added into solution B and stirred for another 30 min at room temperature. The obtained mixture was transferred into a 50 mL Teflon-lined stainless steel autoclave. After 24 h at 180 °C, the autoclave was taken out and the obtained product was washed with DI water three times before freeze-dried in vacuum. The CVO was also prepared according to the similar procedure to CVO-s by using the analytical purity calcium carbonate ($CaCO_3$) as calcium source. 0.008 g of NaCl, 0.013g of $MgCl_2$, 0.093 g of $Al_2(SO_4)_3$, and 0.056g $Fe_2(SO_4)_3$ are added in the CVO to obtain the CVO-d material during the synthesized process.

1.2 Materials Characterizations

The X-ray diffractometer (XRD, Bruker D8 Advance) was applied to characterize the crystal structure range from 5° to 80° with a Cu K α radiation source. HITACHI SU8010 was applied to characterize scanning electron microscope (SEM) and energy dispersive spectroscopy (EDS). The transmission electron microscope (TEM, JEOL JEM-2010) was used to observe microstructure under higher resolution. Thermo Scientific K-Alpha was employed for X-ray photoelectron

spectroscopy (XPS). Thermo Scientific Nicolet iS20 was used to obtain FTIR spectra. Raman spectra was gained by Renishaw Invia RM200. Inductively coupled plasma atomic emission spectroscopy (ICP-MS) was carried out on Aglient 7850.

1.3 Electrochemical Measurements

The CR2032-type coin cells were used to assemble the battery under ambient conditions. The electrodes were prepared by mixing active materials, acetylene black and polyvinylidene fluoride (PVDF) binder with a weight ratio of 7:2:1, which were ground into a slurry using N-methyl pyrrolidone (NMP) as solvent. The slurry was coated on a titanium foil with a diameter of 12 mm and transferred to a vacuum oven for drying at 60 °C for 12 h. The mass loading of active materials was 1.5~2 mg cm^{-2}. Zinc (99.99 %) with the thickness of 0.2 mm was applied as anode while 3 M $Zn(CF_3SO_3)_2$ aqueous solution and glass fiber (GF/D whatman) were used as electrolyte and separator, respectively. The CHI760E electrochemical workstation was used to obtain cyclic voltammetry (CV) curves and electrochemical impedance spectroscopy (EIS). The cycle performance and rate performance of the battery were evaluated by a multi-channel batteries test system (Land CT2001A) with a voltage window of 0.2-1.6 V.

2. Supporting images and tables in the manuscript and their corresponding captions

Table S1 ICP results of the main elements in the shell powder and CVO-s

Element	Shell powder		CVO-s	
	wt (%)	mol g^{-1}	wt (%)	mol g^{-1}
Ca	24.1	0.6025	9.74	0.2435
V	0.0075	0.00015	35.6	0.699
Na	0.85	0.037	0.023	0.001
Mg	0.20	0.0082	0.029	0.0012
Al	0.0595	0.0022	0.0023	0.00009
Fe	0.0576	0.011	0.0068	0.00012

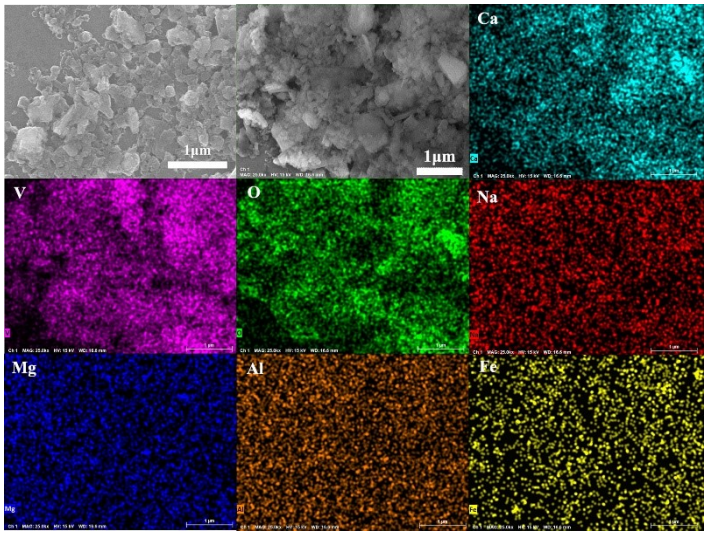

Fig. S1 SEM and its elemental mapping images of the CVO-d material.

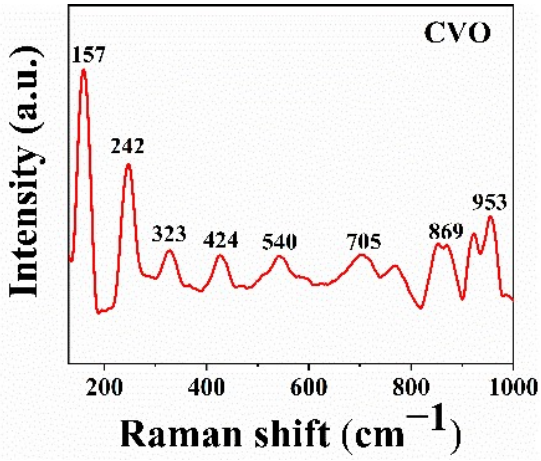

Fig.S2 Raman spectrum of CVO material

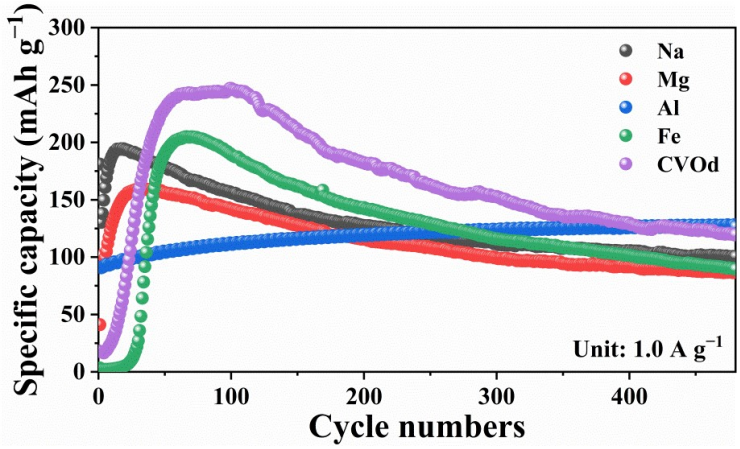

Fig. S3 Cycling performances of batteries with doped elements at 1.0 A g^{-1}.

Introducing substances into layered structure to improve electrochemical performances is a common and effective method in various fields. Some researchers have confirmed this phenomenon. Zhu et. al reported a dissolution-free, stable, low-Zn-preinserted V_2O_5 xerogel

ZIB cathode. Zn^{2+} and structural water as "pillars" and "binder" to stabilize the layered structure of V_2O_5.[1] Wang et. al introduced phenanthroline covalent organic framework in zinc-ion supercapattery.[2] Rashad et. al reported a low-cost method to synthesize $NaV_3O_8 \cdot 1.69H_2O$ nanobelts at room- temperature for Mg batteries.[3]

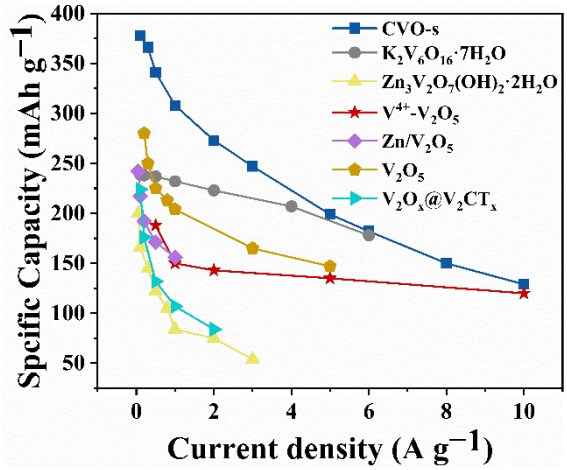

Fig. S4 The contrast diagram of electrochemical performance of CVO-s in our report and those of previously reported V-based cathodes.[4-9]

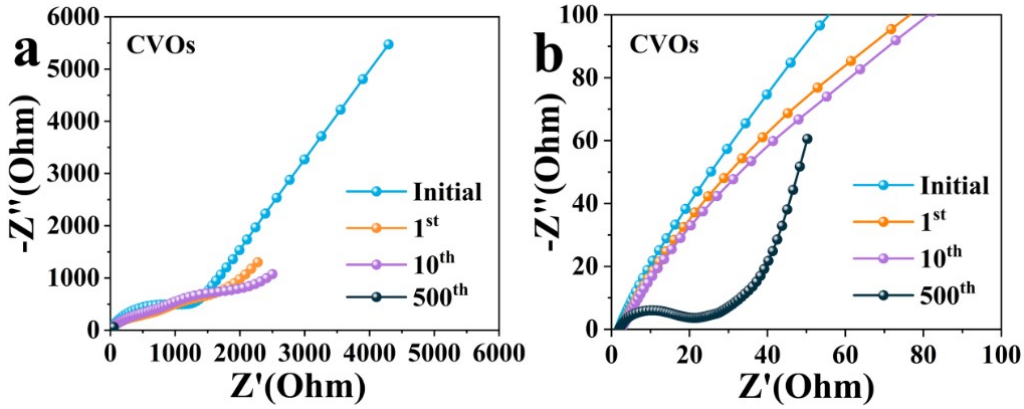

Fig. S5 Nyquist plots of CVO-s at various cycles.

3. Electrochemical reaction mechanism of the cathode materials

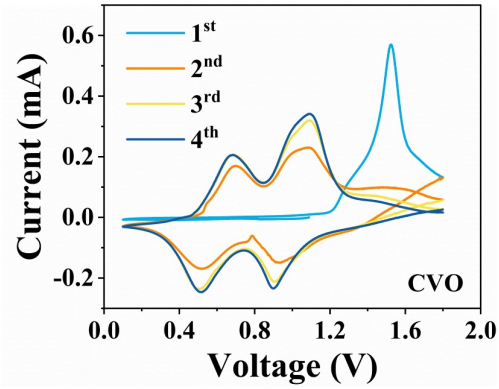

Fig. S6. CV curves of CVO at a scan rate of 0.1 mV s^{-1}.

To investigate the storage mechanism of CVO-s electrode, XRD characterization was carried out through the discharge-charge process. During the first discharging process, most of the diffraction peaks still are attributed to CaV_3O_7, and no other obvious diffraction peaks are observed in Fig. S7a. When the cell is firstly charged to 1.65 V, some new peaks gradually emerge, which can be assigned to $Zn_3(OH)_2(V_2O_7)(H_2O)_2$ (defined as ZVOH, PDF#87-0417) due to the insertion of Zn^{2+} and OH^- from the electrolyte.[10] From Fig. S7b, it can be observed that the CVO-s electrode material turns entirely into ZVOH at the first full-charged state. Even after 1000 cycles, there were no other peaks except for the characteristic peak of ZVOH. However, only characteristic peaks attributed to CaV_3O_7 can be seen in the XRD pattern of CVO electrode after the 1st and 10th cycles. After 1000 cycles, the characteristic peaks of CaV_3O_7 completely disappear and all peaks can be ascribed to ZVOH, which confirms that the CaV_3O_7 in the CVO electrode material is slowly converted into ZVOH along with the continuous cycling. The activation process of ZVOH can be formulated as below: [11-12]

First cycling

$CaV_3O_7 + 6H^+ \rightarrow 3VO^{2+} + CaO + 3H_2O$

$VO^{2+} + H_2O \rightarrow VO_2^+ + 2H^+ + e^-$

$2VO_2^+ + 3Zn^{2+} + 7H_2O \rightarrow Zn_3(OH)_2V_2O_7 \cdot 2H_2O + 8H^+$

(Subsequent cycles)

$Zn_3(OH)_2V_2O_7 \cdot 2H_2O + xZn^{2+} + 2xe^- \leftrightarrow Zn_{3+x}(OH)_2V_2O_7 \cdot 2H_2O$

In order to investigate the electrochemical reaction mechanism of CVO, the CV curves of the CVO electrode are given in Fig. S6. It can be seen that the CV curves of the CVO electrode are very similar to those of the CVO-s electrode, which confirms that CVOs and CVO electrodes should experience the same electrochemical reaction process. At the beginning of the cycles, the amount of the ZVOH in the CVO electrode is low, which has not yet been detected by XRD. However, it can be considered that the formed ZVOH in the CVO electrode materials acts as the active materials in early cyclic reactions and undergoes continuous electrochemical reaction to provide the charge-discharge capacities of the CVO electrode. The continued generation and accumulation of ZVOH are responsible for the continuous capacity growth of the electrode materials.[13] When the continued transformation of CVO into ZVOH is over, the specific capacities of the electrode materials will

reach the maximum value. It is clear that the CVO-s material is easier to transform into ZVOH due to uniform morphology, smaller particle size, superior ion diffusion and electron transport characteristics resulting from doping effect. Therefore, the doping makes the specific capacities of the CVO-s and CVO-d electrode materials will reach the maximum value in a short time. At low current density, the electrolyte has enough time to penetrate deeply into the electrode material, and the cathode material can undergo a deep insertion/exertion process. Therefore, the electrode material has a high internal utilization ratio, which makes the specific capacity of the electrode materials easier to reach the maximum value in a short period.

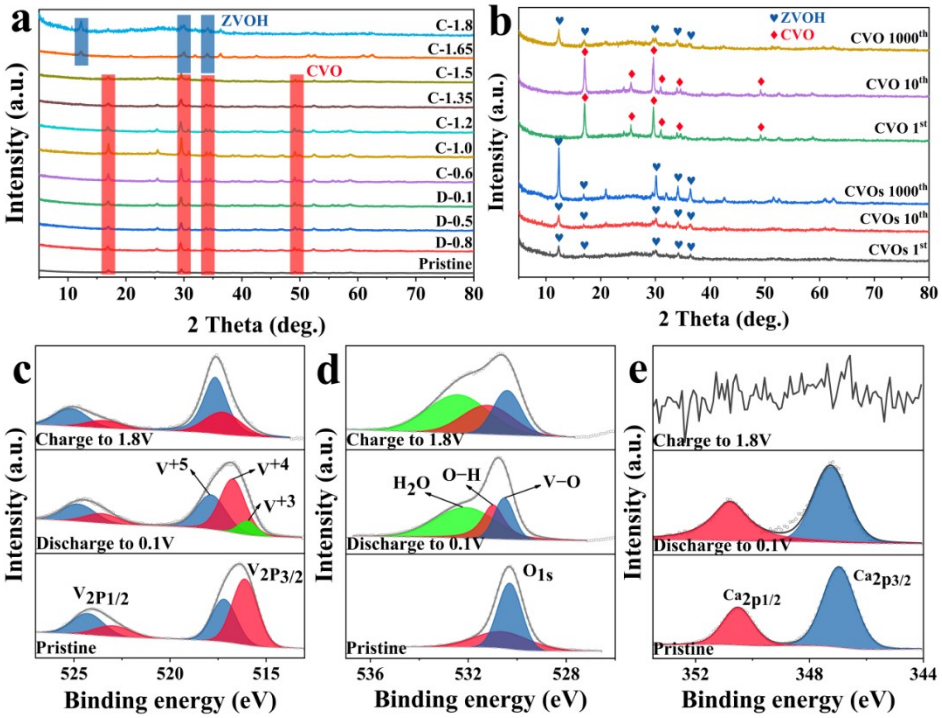

Fig. S7 (a) XRD patterns of CVOs with different voltage states. (b) XRD patterns of CVOs and CVO after 1, 10, and 1000 cycles. X-ray photoelectron spectroscopy (XPS) spectra of CVOs for (c) V, (d) O, and (e) Ca at full-discharge and charge state.

The change of valence state of each element in electrode material is investigated by the XPS spectra in Fig. S7c-e. The change in the valence state for V is given in Fig. S7c. With the intercalation of Zn^{2+} during the discharging process, a new peak belonging to V^{3+} emerges, which is a result of partial reduction of high-valence vanadium to lower valence due to the insertion of Zn^{2+}. When charging to 1.8 V, the peak related to V^{3+} disappears while that related to V^{4+} becomes weak, indicating that V^{4+} and V^{3+} are electrochemically oxidized to V^{5+}. The bonding variations on the O1s spectrum are shown in Fig. S7d. Lattice oxygen (V−O) and physically adsorbed water (O−H) may be detected as two peaks in the initial state, respectively.[14] When discharged to 0.1 V, a broad new peak emerges, which can be attributed to intercalated water molecules.[15] The co-intercalation of Zn^{2+} and H_2O further supports the formation of ZVOH during the subsequent cycles. The XPS spectrum of Ca (Fig. S7e) at the first discharging process indicates the presence of Ca. After charging to 1.8 V, the two peaks belonging to Ca 2p nearly disappear. Such a situation should be due to the intercalation of Zn^{2+} and subsequent replacement of Ca^{2+} on the surface of the CVO-s cathode material, which indicates the structural transformation from CaV_3O_7 to ZVOH, matching

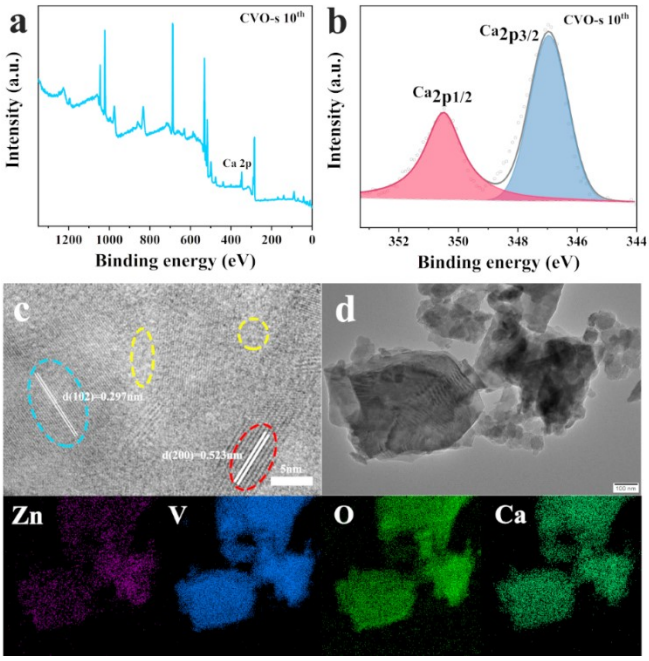

the XRD results in Fig.S7a.

Fig. S8 CVO-s after 10 cycles images of (a-b) XPS spectrum. (c) HRTEM. (d) TEM element mapping.

To further investigate the role and significance of calcium ions in the cathode, the XPS and ICP

of the CVO-s after the 10 cycles were given in Fig. S8a-b and Table S2, which indicate the presence of large amounts of calcium in the electrode material throughout the cycles. The TEM element mapping images (shown Fig. S8d) after the 10 cycles also show Ca are uniformly distributed on the surface of the material. However, after the 10 cycles, all the characteristic peaks in the XRD pattern (shown in 7b) of the CVO-s material are ascribed to $Zn_3(OH)_2(V_2O_7)(H_2O)_2$ (defined as ZVOH, PDF#87-0417) and there are obvious peaks of other substances. Therefore, it can be speculated that calcium ions should be transformed into an amorphous structure in the CVO-s electrode material. The HRTEM images after 10 cycles are given in Fig.S8c, which indicates there are several different diffraction regions. The obvious interlayer distance of 0.297 nm in the blue circle is regarded as the (102) lattice plane of ZVOH. The interlayer distance of 0.523 nm in the red circle can be indexed to (200) plane of CaV_3O_7, indicating the incomplete reaction of CaV_3O_7. Besides, there are some obvious amorphous areas (yellow cycles). Therefore, it is considered that the CaV_3O_7 can gradually change into the ZVOH from the surface of a material to the interior during the cycling process. In the process of the formation of the ZVOH, the calcium ions may be transformed into an amorphous matrix such as CaO. With the continuous transformation of CaV_3O_7 into ZVOH, the formed ZVOH acts as the cathode material and provide the specific capacity of the material, and the inactive amorphous calcium matrix acts as a "spectator" to inhibit the agglomeration of active materials. [12, 16-18] The formation of amorphous matrix enlarges accessible surface area for Zn^{2+} and open Zn^{2+} diffusion pathways, accounting for the initial activation during the cycling.[19-20] This inactive component is benefit to the improvement of electrochemical performance.

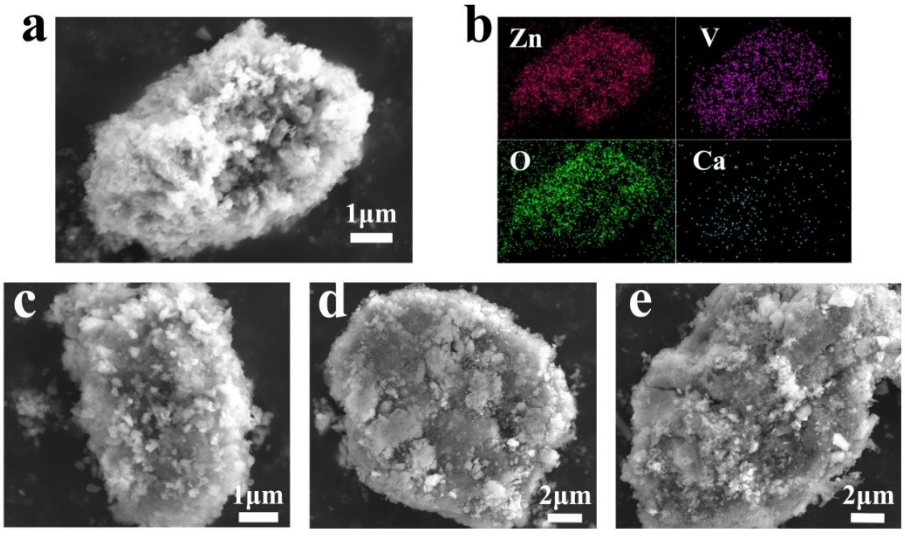

Fig. S9 (a) SEM and (b) elemental mapping images after 1 cycle, SEM images of (c) CVOs after1000 cycles, CVO after (d) 1 cycle and (e) 1000 cycles.

In addition, SEM characterization was used to further study the morphology evolution of the cycled electrodes. After the first cycle, the CVO-s electrode material is made up of uniform and tiny nanoparticles (Fig. 9a), and the uniform distribution of elements in the mapping images also prove the insertion of Zn^{2+} (Fig. S9b). After 1000 cycles, CVO-s electrode material still has the similar morphology (Fig. S9c), demonstrating obvious structural stability during continuous cycling process. Compared with the CVO-s, the CVO electrode is mainly composed of large block particles in addition to some tiny particles (Fig. S9d-e). It is clear that the uniform and fine nanoparticles formed after electrochemical conversion are more conducive to reversible electrochemical reaction, thus ensuring excellent electrochemical performance of electrode materials.

Table S2 ICP results of the main elements CVO-s after 10 cycles

Element	wt (%)	mol g^{-1}
Ca	7.055	0.176
V	22.245	0.436
Zn	4.272	0.066

References

1 K. Zhu, T. Wu, W. Bergh, M. Stefik, K. Huang, *ACS Nano*, 15, 2021, 6 10678-10688.

2 W. Wang, V. Kale, Z. Cao, S. Kandambeth, W. Zhang, J. Ming, P. Parvatkar, E. Abou-Hamad, O. Shekhah, L. Cavallo, M. Eddaoudi, H. Alshareef, *ACS Energy Lett*., 5, 2020, 7 2256-2264.

3 M. Rashad, H. Zhang, M. Asif, K. Feng, X. Li, H. Zhang, *ACS Appl. Mater. Interfaces*, 10, 2018, 5 4757-4766.

4 B. Sambandam, V. Soundharrajan, S. Kim, M. Alfaruqi, J. Jo, S. Kim, V. Mathew, Y. Sun, J. Kim, *J. Mater. Chem. A*, 2018, 6 15530-15539.

5 C. Xia, J. Guo, Y. Lei, H. Liang, C. Zhao, H. N. Alshareef, *Adv. Mater*., 30, 2018, 5 1705580.

6 F. Liu, Z. Chen, G. Fang, Z. Wang, Y. Cai, B. Tang, J. Zhou, S. Liang, *Nano-Micro Lett*., 25, 2019,11.

7 P. Hu, M. Yan, T. Zhu, X. Wang, X. Wei, J. Li, L. Zhou, Z. Li, L. Chen, L. Mai, *ACS Appl. Mater. Inter*., 9, 2017, 49 42717-42722.

8 H. Qin, L. Chen, L. Wang, X. Chen, Z. Yang, *Electrochim. Acta*, 306, 2019, 20 307-316.

9 R. Venkatkarthick, N. Rodthongkum, X. Zhang, S. Wang, P. attananuwat, Y. Zhao, R. Liu, J. Qin, *ACS Appl. Energy Mater*., 3, 2020, 5 4677-4689.

10 Z. Pang, B. Ding, J. Wang, Y. Wang, L. Xu, L. Zhou, X. Jiang, X. Yan, J.P. Hill, L. Yu, Y. Yamauchi, *Chem. Eng. J*., 2020 446.

11 Y. Li, W. Yang, W. Yang, Y. Huang, G. Wang, C. Xu, F. Kang, L. Dong, *J. Energy Chem*. 60, 2021 233–240

12 X. Xu, C. Niu, M. Duan, X. Wang, L. Huang, J. Wang, L. Pu, W. Ren, C. Shi, J. Meng, B. Song, L. Mai, *Nat. Commun*. 8 2017 460.

13 S. Cai, Y. Wu, H. Chen, Y. Ma, T. Fan, M. Xu, S. Bao, *J. Colloid Interf*. Sci. 2022, 615, 30–37,

14 F. Zhang, M. Du, Z. Miao, H. Li, W. Dong, Y. Sang, H. Jiang, W. Li, H. Liu, S. Wang, *InfoMat*.,2022.

15 Y. Du, X. Wang, Y. Zhang, H. Zhang, J. Man, K. Liu, J. Sun, *Chem. Eng. J*., 2022, 434.

16 P. Wu, X. Xu, Y. Wu, F. Xu, X. Wang, J. Meng, C. Han, X. Liu, Z. Zhu and L. Mai, *Adv. Energy Mater*. 11, 2021, 2003612.

17 C. Han, X. Zhang, X. Xu, Q. Li, Q. He, J. Meng, X. Wang, Z. Liu, P. Wu and L. Mai, *Nanoscale*, 10, 2018, 12963–12969.

18 M. V. Reddy, G. V. Subba Rao, and B. V. R. Chowdari, *Chem. Rev*. 13, 2013, 5364−5457.

19 J. Huang, H. Liang, Y. Tang, B. Lu, J. Zhou and S. Liang, *Adv. Energy Mater*. 12, 2022, 2201434.

20 J. K. Shon, H. S. Lee, G. O. Park, J. Yoon, E. Park, G. S. Park, S. S. Kong, M. Jin, J. M. Choi, H. Chang, S. Doo, J. M. Kim, W. S. Yoon, C. Pak, H. Kim, G. D. Stucky, *Nat. Commun*. 7, 2016, 7 11049.